ACS Photonics

pubs.acs.org/journal/apchd5

Article

Terahertz Nonlinear Spectroscopy of Water Vapor

Payman Rasekh,* Akbar Safari,* Murat Yildirim, Ravi Bhardwaj, Jean-Michel Ménard, Ksenia Dolgaleva, and Robert W. Boyd

Cite This: *ACS Photonics* 2021, 8, 1683−1688

Read Online

ACCESS | Metrics & More | Article Recommendations

ABSTRACT: The water molecule has millions of rotational transitions in the infrared and terahertz region, and the resulting absorption features dominate the transmission spectrum of atmospheric terahertz measurements, even for propagation distances as short as tens of centimeters. Remarkably, we observe that the absorption at the position of these resonances increases with the THz intensity. We explain this observation by stepwise multiphoton transitions in water molecules. The estimated value of the effective third-order susceptibility is extremely large: $\chi^{(3)} = (0.4 + 6i) \times 10^2$ m^2/V^2. We note for comparison that the value of $\chi^{(3)}$ for fused silica at optical frequencies is on the order of 10^{-22} m^2/V^2. Furthermore, our results provide new insight into the various transitions of the water molecule and their nonlinear response to electromagnetic radiation, paving the way to more accurate THz spectroscopy, imaging, and sensing systems, thereby facilitating future emerging THz technologies.

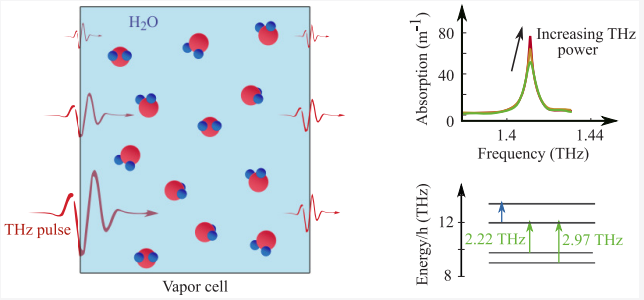

KEYWORDS: *terahertz, nonlinear optics, water vapor, two-level-system approximation, reverse saturation of absorption*

Water vapor pervades the atmosphere of the Earth and exhibits absorption in a broad frequency range of the electromagnetic spectrum, associated with rotational, as well as inter- and intramolecular vibrational transitions.[1,2] The absorption spectrum of water vapor reflects its molecular structure and, therefore, can be used as a spectroscopic fingerprint for its detection and identification. This spectrum is, however, very complex and highly rich in resonances, which have been the center of intense spectroscopic investigations for many decades.[3−6] Moreover, atmospheric water vapor is responsible for almost all the spectral modifications of electromagnetic radiation from 0.5 to 20 THz.[7] It is, therefore, crucial to gain a better understanding of these resonances, especially in the context of high field excitation due to an increasing demand for high power sources to enable numerous emerging THz applications.

Indeed, THz-based systems are finding a niche in fields such as information and communication technology,[8] spectroscopy and imaging,[9−11] and ultrafast control,[12] as well as biomedicine.[13,14] In addition, long-path THz time-domain spectroscopy in the open air is realized to demonstrate the potential of line-of-sight THz communications,[15,16] THz sensing,[17] monitoring pollutants and dangerous gases,[18] nondestructive evaluation,[19] global environmental monitoring,[20] and THz imaging through the fog and smoke,[21] which often require propagation of intense THz pulses through the atmosphere. Therefore, studying the nonlinear response of water vapor in the THz domain not only provides insight into the intermolecular structure of water vapor, but also represents great importance for practical applications.

With the coherent generation and detection of THz radiation, it is possible to measure not only absorption spectra with high spectral resolution, but also the dispersive response of water vapor simultaneously.[22] With recent developments in coherent THz radiation sources, phase-locked THz pulses with higher intensities are becoming routinely accessible.[23] As a consequence, THz science has been engaged in studying the nonlinear response of different materials in the THz region of the spectrum; examples include nonlinear response of free electrons to single-cycle THz pulses,[24] THz-induced carrier multiplication via impact ionization,[25−27] and THz saturable absorption and high-harmonic generation by hot electrons.[28−33] Moreover, it has been shown that the Kerr-type nonlinearity of dense materials such as solids[23,34−36] and liquids[37,38] is typically larger than their Kerr-type nonlinear response in the optical domain. However, unlike solids and liquids, gaseous materials such as water vapor can have sharp

Received: January 11, 2021
Published: May 25, 2021

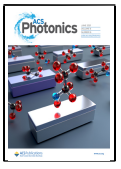

https://doi.org/10.1021/acsphotonics.1c00056
ACS Photonics 2021, 8, 1683−1688

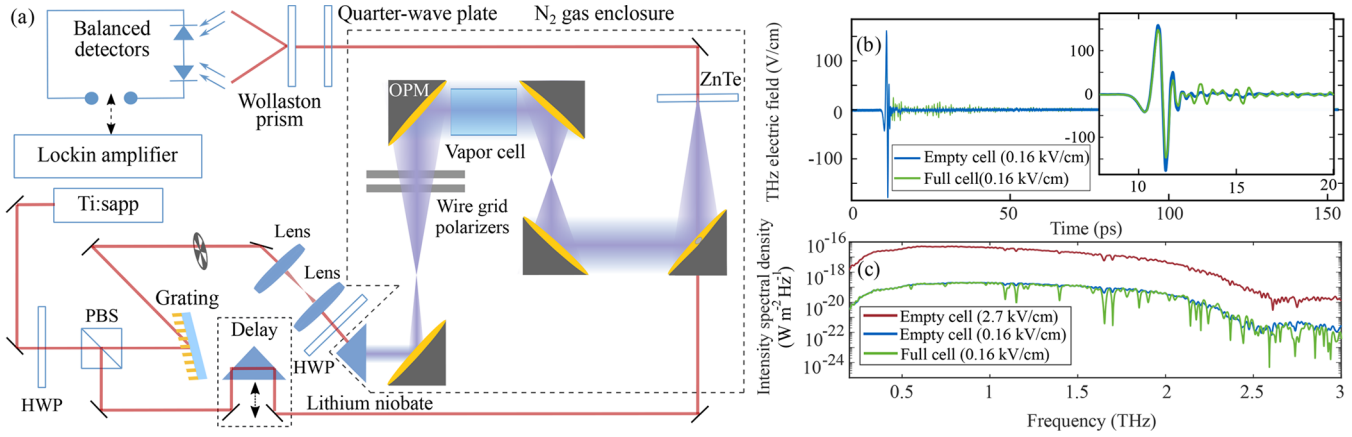

Figure 1. (a) Experimental setup diagram for THz generation and detection. The vapor cell is placed between two parabolic mirrors where the THz beam is collimated. A half-wave plate (HWP) and a polarizing beam splitter (PBS) are used to split the pump and probe beams. OPM is off-axis parabolic mirror. (b) Detected THz field at the lowest power as a function of time. The blue and green lines represent the detected fields in the absence and presence of water vapor, respectively. The inset enlarges the main peaks and the trailing oscillations. (c) Intensity spectral density with and without water vapor calculated from the Fourier transform of the time-domain signals. The THz spectrum extends to 2.5 THz, but we focus on the resonances between 1 and 1.5 THz, where the signal-to-noise ratio of the source is maximum.

resonances in the THz range, and the Kerr-type nonlinear response of these transitions has not been studied to date.

In this Article, we report on the nature of nonlinear interactions of THz pulses with atmospheric water vapor at different THz pulse intensities. First, we measure the linear response of water vapor and explain our results by comparing them with theoretical predictions. Then, we perform nonlinear THz time-domain spectroscopy (THz-TDS) to show how increasing the electric field intensity of the THz radiation modifies the absorption and dispersion of the vapor. In contrast to two-level atomic systems, where the absorption decreases with increasing field intensity, we observe an increase in absorption for some of the transitions. The observed reverse-saturation of absorption is explained based on stepwise multiphoton transitions. Furthermore, we show that the THz field experiences an extremely large nonlinear refractive index at frequencies near to the resonances of water molecules.

EXPERIMENTAL DETAILS

The THz field is generated using optical rectification in a lithium niobate crystal with the tilted-pulse-front technique.[39] In the generation arm (Figure 1a), we use an 800 nm, 45 fs Ti:sapphire pulsed laser beam that diffracts from a grating that is used to introduce the required tilt to the intensity front of the pulse and to fulfill the phase matching condition of the nonlinear-induced polarization in the lithium niobate. The pump beam is vertically polarized with a power of 300 mW measured before the crystal. After the second cylindrical lens, we spatially filter the diffracted near-infrared laser beam to remove the unwanted diffraction orders and to generate a THz beam with a smooth near-Gaussian transverse profile. Off-axis gold parabolic mirrors are used to collimate and expand the THz radiation. Also, a pair of free-standing wire-grid polarizers is used after the first parabolic mirror to control the intensity of the THz beam without introducing dispersion to the transmitted field.

In the detection arm, both the THz beam transmitted through the vapor cell and a near-infrared probe pulse overlap at the focal position into a 200 μm thick ZnTe crystal. In the absence of a THz electric field, a quarter-wave plate converts the vertical polarization of the probe beam into a circular polarization. When the THz beam copropagates with the probe beam, the THz field modifies the optical refractive index seen by the probe pulse by means of the linear electro-optic (Pockels) effect, thereby inducing an ellipticity to the probe's polarization. We measure this ellipticity as a function of time delay with respect to the THz pulse in order to determine the time dependence of the THz field. A Wollaston prism along with a pair of balanced photodetectors and a lock-in amplifier allow for a linear detection of the induced birefringence at the chopping frequency of the probe. The peak of the electric field at the detection crystal is calculated based on the modulation of the balanced photodetectors using the procedure given in ref 40 and is then rescaled proportional to the beam diameters to obtain the peak electric field at the location of the vapor cell. We estimate the maximum peak value of the THz electric field to be ≈2.7 kV/cm at the location of the vapor cell. The THz part of the setup is enclosed and purged with dry nitrogen to prevent unwanted absorption from water vapor.

The water vapor cell is a cylinder with a length of 8 cm and a diameter of 5.5 cm. To avoid absorption and reflection of the THz field, ultrathin cling wraps are used as the windows of the cell.[41] The vapor cell is placed in the collimated arm of the THz field and filled with dry nitrogen under atmospheric pressure. A few drops of distilled water are placed inside the cell to provide the required water vapor and a relative humidity of 100%. A heating wire wrapped around the cell and a thermocouple are used to keep the temperature of the vapor cell at T = 309 K. To determine the effect of water vapor on the transmitted field, we collect the data with and without the water vapor. We repeat the measurements at different THz field amplitudes by rotating the first wire-grid polarizer while keeping the second one fixed to maintain a constant polarization state.

RESULTS AND DISCUSSION

Figure 1b shows the time-domain signals for the lowest THz amplitude corresponding to 162 V/cm, where a linear response of water vapor is expected. The effect of the sharp resonances of the water vapor appears as the trailing oscillations due to the free induction decay of the resonances. A long scan time of 155 ps is used during the measurements in order to collect as much

https://doi.org/10.1021/acsphotonics.1c00056
ACS Photonics 2021, 8, 1683−1688

spectral information as possible. The spectral density of the THz field is shown in Figure 1c where the fast Fourier transform (FFT) of the temporal shape is displayed. The zero-padding technique[42] is applied on the temporal signal to achieve a smoother interpolation in the frequency domain.

For this study, we focused our attention on the spectral region between 1 and 1.5 THz where water vapor exhibits six strong resonances and where our THz system features an optimal signal-to-noise ratio. The linear susceptibility of the vapor due to these six resonances is given by

$$\chi = \chi_R + i\chi_I = \sum_{j=1}^{6} \frac{c^2}{2\pi^2 \nu_j} \frac{\nu_j - \nu + i\gamma_j}{\gamma_j^2 + (\nu_j - \nu)^2} n_w S_j \quad (1)$$

where c is the speed of light in cm/s, $n_w = 1.389 \times 10^{18}$ cm^{-3} is the number density of the water molecules and ν_j is the resonant frequency of the jth transition. The line width of each transition depends on the temperature T according to

$$\gamma_j = c\left(\frac{296}{T}\right)^{a_j} (\gamma_s P_w + \gamma_f P_f) \quad (2)$$

where a_j is the temperature exponent for the air broadening, and $P_w \approx 0.058$ and $P_f \approx 0.985$ are the partial pressures of the water vapor and the nitrogen gas in the cell calculated from Antoine formula.[43] The self-broadening and foreign gas broadening coefficients of these six transitions are approximately the same and are found to be $\gamma_s = 0.5$ and $\gamma_f = 0.1$ cm^{-1} atm^{-1}, respectively. The required parameters are extracted from the HITRAN database[44,45] and are listed in Table 1.

Table 1. Transition Parameters of the Six Strongest Resonances of Water Vapor Molecules in the Spectral Range between 1 and 1.5 THz[a]

j	ν_j (THz)	a_j	γ_j (GHz)	A_j (s^{-1})	g_j''	$S_j \times 10^{20}$ (cm/molecule)
1	1.0974	0.78	3.91	0.0164	21	15.18
2	1.1133	0.79	3.40	0.0184	3	4.521
3	1.1629	0.78	3.70	0.0227	21	16.67
4	1.2076	0.81	3.49	0.0283	9	5.308
5	1.2288	0.76	3.73	0.0187	5	4.421
6	1.4106	0.80	3.70	0.0426	33	13.87

[a]The vapor cell is at $T = 309°$ K and contains 1 atm of nitrogen gas. ν_j and γ_j are the central frequency and the line width, a_j is the air broadening exponent, A_j is the Einstein A coefficient, g_j'' is the degeneracy factor of the excited state, and S_j is the spectral line intensity of the jth transition.

The spectral line intensity for each transition S_j is a function of temperature. In thermodynamic equilibrium, the population distribution between the energy levels is governed by Boltzman statistics and changes with temperature. Therefore, the spectral line intensity for each transition can be calculated from[46]

$$S_j = \frac{A_j c}{8\pi\nu_j^2} \frac{g_j'' e^{-h\nu_j/k_B T}(1 - e^{-h\nu_j/k_B T})}{\sum_k g_k e^{-h\nu_j/k_B T}} \quad (3)$$

where A_j is the Einstein A coefficient and g_j'' is the degeneracy factor of the excited state (Table 1). h and k_B are Planck and Boltzmann constants, respectively. The sum in the denominator of eq 3 represents the total internal partition sum and can be found in the HITRAN database for water molecules.[44]

The last column of Table 1 shows the spectral line intensities at $T = 309$ K calculated from eq 3.

In Figure 2, we plot the calculated (linear response) and experimentally measured absorption coefficients. We notice

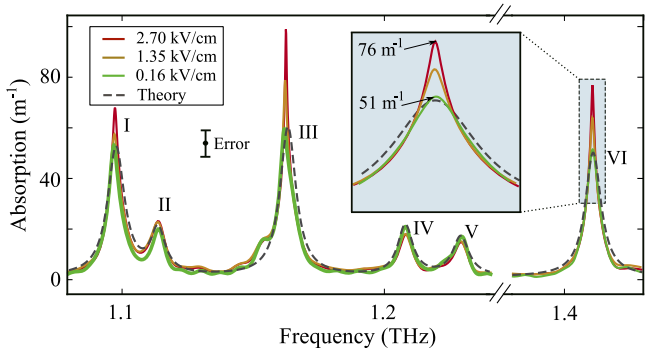

Figure 2. Absorption coefficient of water vapor at temperature $T = 309$ K. The absorption peaks are numbered from I to VI, and the corresponding labels are shown next to each peak. While the absorption of the lowest-intensity signals fits well with the linear model, the absorption at the resonances I, III, and VI increases with the intensity. The error bar is two times the standard deviation for a measurement repeated four times.

that, for the lowest intensity signal, the absorption coefficient fits well with the linear theoretical model. However, as the strength of the field increases, there is a consistent increase in the absorption at the location of the resonances I, III, and VI. This change is an indication of the nonlinear process associated with stepwise multiphoton absorption.

With a two-level-system approximation, one expects to see saturation of the transition, and thus, a decrease in absorption as the intensity increases. However, Figure 2 clearly shows that absorption of water molecules at some resonances increases with intensity, which indicates that two-level approximation is not valid here. In Figure 3, we plot the rotational energy levels of water molecules relevant to the six transitions in our study. The blue arrows show the transitions corresponding to the six resonances shown in Figure 2. As can be seen, transition V populates the ground state of transition I, which consecutively

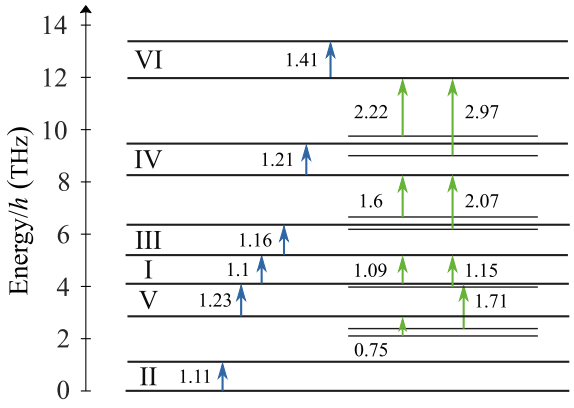

Figure 3. Rotational energy level diagram of water vapor taken from HITRAN.[46] The blue arrows show the six transitions under study between 1 and 1.5 THz, labeled from I to VI. The green arrows on the right indicate other transitions that affect the population of the levels relevant to our study. The number beside each arrow indicates the frequency of the transition in THz.

https://doi.org/10.1021/acsphotonics.1c00056
ACS Photonics 2021, 8, 1683−1688

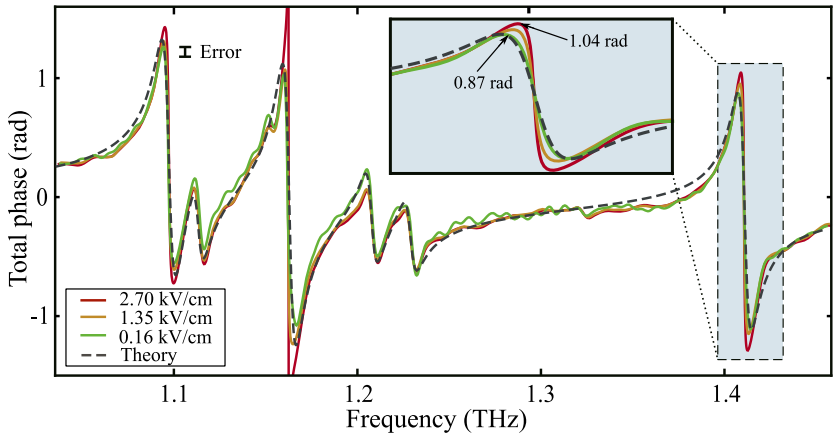

Figure 4. Overall phase of the transmitted THz field, including linear and nonlinear contributions, as a function of frequency. As the intensity of the field increases, the amplitude of the phase in the vicinity of the resonances increases as well. The error bar is two times the standard deviation for a measurement repeated four times.

populates the ground state of transition III. Therefore, a large increase in the absorption of the third transition is expected as its ground state population increases with THz field intensity. Moreover, the THz field has a broad spectrum (≈1 THz full width at half-maximum) covering the frequency window from 0 to 2.5 THz that excites many other transitions, as can be seen in Figure 1c. The excited state of some of these transitions are indeed the ground state of one of the six transitions in our study. These transitions are shown by the green arrows in Figure 3. For example, the ground state of the sixth transition is pumped by two other transitions at 2.2 and 2.97 THz.

Since we use a coherent detection technique, we are also able to retrieve the spectral phase information on the THz field from the Fourier analysis. Figure 4 shows the phase of the THz field after the vapor cell as a function of frequency. The theoretical linear model fits well with the phase of the lowest-intensity signal, which is expected to be linear. Nonlinear response of the material can be found where the higher-intensity signal acquires additional phase shift, specifically, at the location of the water vapor resonances. This nonlinear phase shift can be understood again from stepwise multiphoton transitions and pumping of the ground states of different transitions by the broadband THz pulse, as explained earlier.

Assigning an effective third-order nonlinear susceptibility to the transitions would allow one to perceive the strength of the nonlinearity by comparing it with that of other materials. We consider the sixth transition in Figure 2. We focus on the effective third-order susceptibility given by $\chi^{(3)}(\nu: \nu_p + \nu - \nu_p)$, where $\nu = 1.41$ THz is the frequency of the sixth transition and ν_p indicates the pump field at 2.2 THz (see Figure 3). The effect of pumping by the other transition at 2.97 THz is ignored, because the spectral density of our THz source is negligible at that frequency. The imaginary part of $\chi^{(3)}$ is related to the total absorption coefficient defined by $\alpha = \alpha_0 + \beta I_p$, where $\alpha_0 = 51\ m^{-1}$ is the linear absorption coefficient, β is the two-photon absorption (TPA) coefficient, and I_p is the intensity of the pump. At the maximum THz power, the intensity of the pump within the THz line width is $I_p = 7 \times 10^{-9}$ W/m^2, and the absorption coefficient is $\alpha = 76 \pm 5\ m^{-1}$ (see Figure 2). Therefore, the TPA coefficient is $\beta = (3.5 \pm 0.7) \times 10^{20}$ cm/GW, from which the imaginary part of $\chi^{(3)}$ is found to be $\chi_I^{(3)} = (6 \pm 1) \times 10^2\ m^2/V^2$.

The real part of $\chi^{(3)}$ can be found from the nonlinear refractive index $n_2 = \Delta\phi/(kLI_p)$,[47] where L is the length of the cell, k is the wavenumber, and $\Delta\phi = 0.17$ radians is the nonlinear phase shift of the sixth transition, as shown in Figure 4. We calculate the value of the nonlinear refractive index to be $n_2 = (1 \pm 0.3) \times 10^4\ m^2/W$; thus, the real part of $\chi^{(3)}$ is $\chi_R^{(3)} = (0.4 \pm 0.1) \times 10^2\ m^2/V^2$.

CONCLUSION

We observed an extremely large nonlinear response of water vapor in the THz regime. We attributed this large nonlinearity to stepwise multiphoton transitions in water molecules and estimated an effective third-order susceptibility of $\chi^{(3)} = (0.4 + 6i) \times 10^2\ m^2/V^2$. Time-domain spectroscopy has been used widely to measure the absorption spectrum of water vapor in the THz regime. However, our results show that optical pumping of subsequent transitions can modify the observed spectrum even at low intensities. A primary obstacle to many THz applications is the attenuation of the field by water vapor in the atmosphere. A naïve approach to overcome this problem is to increase the THz intensity to saturate the transition and reduce the absorption. However, our study shows that, as the intensity increases, the absorption of many resonant lines increases as well. Moreover, nonlinear spectroscopy provides valuable information on the transitions and the energy levels of the molecules. Thus, our work paves the way for a better understanding of water vapor molecular structure, to validate the rotational energy levels of water molecules and to study the role of water clusters in the absorption spectrum.[48−52]

AUTHOR INFORMATION

Corresponding Authors

Payman Rasekh − *School of Electrical Engineering and Computer Science, University of Ottawa, Ottawa, Ontario K1N 6N5, Canada*; orcid.org/0000-0002-0708-7554; Email: p.rasekh@gmail.com

Akbar Safari − *Department of Physics, University of Ottawa, Ottawa, Ontario K1N 6N5, Canada*; Email: akbar.safari@gmail.com

Authors

Murat Yildirim − *Department of Physics, University of Ottawa, Ottawa, Ontario K1N 6N5, Canada*

https://doi.org/10.1021/acsphotonics.1c00056
ACS Photonics 2021, 8, 1683−1688

Ravi Bhardwaj − *Department of Physics, University of Ottawa, Ottawa, Ontario K1N 6N5, Canada*
Jean-Michel Ménard − *Department of Physics, University of Ottawa, Ottawa, Ontario K1N 6N5, Canada*
Ksenia Dolgaleva − *School of Electrical Engineering and Computer Science, University of Ottawa, Ottawa, Ontario K1N 6N5, Canada; Department of Physics, University of Ottawa, Ottawa, Ontario K1N 6N5, Canada*
Robert W. Boyd − *School of Electrical Engineering and Computer Science, University of Ottawa, Ottawa, Ontario K1N 6N5, Canada; Department of Physics, University of Ottawa, Ottawa, Ontario K1N 6N5, Canada; Institute of Optics, University of Rochester, Rochester, New York 14627, United States;* orcid.org/0000-0002-1234-2265

Complete contact information is available at: https://pubs.acs.org/10.1021/acsphotonics.1c00056

Notes

The authors declare no competing financial interest.

■ ACKNOWLEDGMENTS

This work was supported by the Canada Excellence Research Chairs program, Canada Research Chairs program and the National Science and Engineering Research Council of Canada (NSERC) Discovery and Strategic programs. R.W.B. also thanks the US Army Research Office and the Office of Naval Research for their support.

■ REFERENCES

(1) Deepak, A.; Wilkerson, T. D.; Ruhnke, L. H. *Atmospheric Water Vapor*; Academic Press: New York, 1980, DOI: DOI: 10.1016/C2013-0-10573-9.
(2) Slocum, D. M.; Slingerland, E. J.; Giles, R. H.; Goyette, T. M. Atmospheric absorption of terahertz radiation and water vapor continuum effects. *J. Quant. Spectrosc. Radiat. Transfer* **2013**, *127*, 49.
(3) Horvath, H. Atmospheric light absorption - A review. *Atmos. Environ., Part A* **1993**, *27*, 293.
(4) Mecke, R. Das Rotationsschwingungsspektrum des Wasserdampfes. *Eur. Phys. J. A* **1933**, *81*, 313.
(5) Elsasser, W. M. Far Infrared Absorption of Atmospheric Water Vapor. *Astrophys. J.* **1938**, *87*, 497.
(6) Savolainen, J.; Ahmed, S.; Hamm, P. Two-dimensional Raman-terahertz spectroscopy of water. *Proc. Natl. Acad. Sci. U. S. A.* **2013**, *110*, 20402.
(7) Kemp, A. J.; Birch, J. R.; Afsar, M. N. The refractive index of water vapour: A comparison of measurement and theory. *Infrared Phys.* **1978**, *18*, 827.
(8) Kleine-Ostmann, T.; Nagatsuma, T. A Review on Terahertz Communications Research. *J. Infrared, Millimeter, Terahertz Waves* **2011**, *32*, 143.
(9) Dong, J.; Locquet, A.; Melis, M.; Citrin, D. Global mapping of stratigraphy of an old-master painting using sparsity-based terahertz reflectometry. *Sci. Rep.* **2017**, *7*, 15098.
(10) Kaltenecker, K. J.; et al. Ultrabroadband perfect imaging in terahertz wire media using single-cycle pulses. *Optica* **2016**, *3*, 458.
(11) Federici, J. F.; et al. THz imaging and sensing for security applications—explosives, weapons and drugs. *Semicond. Sci. Technol.* **2005**, *20*, S266.
(12) Bowlan, P.; et al. Probing and controlling terahertz-driven structural dynamics with surface sensitivity. *Optica* **2017**, *4*, 383.
(13) Brun, M.-A.; et al. Terahertz imaging applied to cancer diagnosis. *Phys. Med. Biol.* **2010**, *55*, 4615.
(14) Smolyanskaya, O.; et al. Glycerol dehydration of native and diabetic animal tissues studied by thz-tds and nmr methods. *Biomed. Opt. Express* **2018**, *9*, 1198.
(15) Moon, E.-B.; Jeon, T.-I.; Grischkowsky, D. R. Long-Path THz-TDS Atmospheric Measurements Between Buildings. *IEEE Trans. Terahertz Sci. Technol.* **2015**, *5*, 742.
(16) Kim, G.-R.; Jeon, T.-I.; Grischkowsky, D. R. 910-m propagation of THz ps pulses through the Atmosphere. *Opt. Express* **2017**, *25*, 25422.
(17) Brucherseifer, M.; Nagel, M.; Haring Bolivar, P.; Kurz, H.; Bosserhoff, A.; Buttner, R. Label-free probing of the binding state of DNA by time-domain terahertz sensing. *Appl. Phys. Lett.* **2000**, *77*, 4049.
(18) Hsieh, Y.-D.; Nakamura, S.; Abdelsalam, D. G.; Minamikawa, T.; Mizutani, Y.; Yamamoto, H.; Iwata, T.; Hindle, F.; Yasui, T. Dynamic terahertz spectroscopy of gas molecules mixed with unwanted aerosol under atmospheric pressure using fibre-based asynchronous-optical-sampling terahertz time-domain spectroscopy. *Sci. Rep.* **2016**, *6*, 28114.
(19) Stoik, C. D.; Bohn, M. J.; Blackshire, J. L. Nondestructive evaluation of aircraft composites using transmissive terahertz time domain spectroscopy. *Opt. Express* **2008**, *16*, 17039.
(20) Sengupta, K. Silicon-Based Terahertz Circuits and Systems. *Dissertation (Ph.D.)*, California Institute of Technology, 2012, DOI: 10.7907/MBXB-6R29.
(21) Yang, Y.; Mandehgar, M.; Grischkowsky, D. R. Broadband THz Signals Propagate Through Dense Fog. *IEEE Photonics Technol. Lett.* **2015**, *27*, 383.
(22) Yang, Y.; Mandehgar, M.; Grischkowsky, D. R. Understanding THz Pulse Propagation in the Atmosphere. *IEEE Trans. Terahertz Sci. Technol.* **2012**, *2*, 406.
(23) Hebling, J.; Yeh, K.-L.; Hoffmann, M. C.; Nelson, K. A. High-Power THz Generation, THz Nonlinear Optics, and THz Nonlinear Spectroscopy. *IEEE J. Sel. Top. Quantum Electron.* **2008**, *14*, 345.
(24) Turchinovich, D.; Hvam, J. M.; Hoffmann, M. C. Self-phase modulation of a single-cycle terahertz pulse by nonlinear free-carrier response in a semiconductor. *Phys. Rev. B: Condens. Matter Mater. Phys.* **2012**, *85*, 201304.
(25) Tarekegne, A. T.; Iwaszczuk, K.; Zalkovskij, M.; Strikwerda, A. C.; Jepsen, P. U. Impact ionization in high resistivity silicon induced by an intense terahertz field enhanced by an antenna array. *New J. Phys.* **2015**, *17*, 043002.
(26) Tani, S.; Blanchard, F.; Tanaka, K. Ultrafast Carrier Dynamics in Graphene under a High Electric Field. *Phys. Rev. Lett.* **2012**, *109*, 166603.
(27) Lange, C.; et al. Extremely nonperturbative nonlinearities in gaas driven by atomically strong terahertz fields in gold metamaterials. *Phys. Rev. Lett.* **2014**, *113*, 227401.
(28) Gaal, P.; et al. Nonlinear Terahertz Response of n-Type GaAs. *Phys. Rev. Lett.* **2006**, *96*, 187402.
(29) Chai, X.; et al. Subcycle Terahertz Nonlinear Optics. *Phys. Rev. Lett.* **2018**, *121*, 143901.
(30) Hwang, H. Y.; et al. Nonlinear thz conductivity dynamics in p-type cvd-grown graphene. *J. Phys. Chem. B* **2013**, *117*, 15819.
(31) Razzari, L.; et al. Nonlinear ultrafast modulation of the optical absorption of intense few-cycle terahertz pulses in n-doped semiconductors. *Phys. Rev. B: Condens. Matter Mater. Phys.* **2009**, *79*, 193204.
(32) Hafez, H. A.; et al. Extremely efficient terahertz high-harmonic generation in graphene by hot dirac fermions. *Nature* **2018**, *561*, 507.
(33) Schubert, O.; et al. Sub-cycle control of terahertz high-harmonic generation by dynamical Bloch oscillations. *Nat. Photonics* **2014**, *8*, 119.
(34) Zalkovskij, M.; et al. Terahertz-induced Kerr effect in amorphous chalcogenide glasses. *Appl. Phys. Lett.* **2013**, *103*, 221102.
(35) Dolgaleva, K.; Materikina, D. V.; Boyd, R. W.; Kozlov, S. A. Prediction of an extremely large nonlinear refractive index for crystals at terahertz frequencies. *Phys. Rev. A: At., Mol., Opt. Phys.* **2015**, *92*, 023809.
(36) Rasekh, P.; et al. Propagation of broadband THz pulses: effects of dispersion, diffraction and time-varying nonlinear refraction. *Opt. Express* **2020**, *28*, 3237.

(37) Hoffmann, M. C.; Brandt, N. C.; Hwang, H. Y.; Yeh, K.-L.; Nelson, K. A. Terahertz Kerr effect. *Appl. Phys. Lett.* **2009**, *95*, 231105.
(38) Tcypkin, A. N.; et al. High Kerr nonlinearity of water in THz spectral range. *Opt. Express* **2019**, *27*, 10419.
(39) Hebling, J.; Yeh, K.-L.; Hoffmann, M. C.; Bartal, B.; Nelson, K. A. Generation of high-power terahertz pulses by tilted-pulse-front excitation and their application possibilities. *J. Opt. Soc. Am. B* **2008**, *25*, B6.
(40) Blanchard, F.; et al. Generation of 1.5 μJ single-cycle terahertz pulses by optical rectification from a large aperture ZnTe crystal. *Opt. Express* **2007**, *15*, 13212.
(41) van Exter, M.; Fattinger, C.; Grischkowsky, D. Terahertz time-domain spectroscopy of water vapor. *Opt. Lett.* **1989**, *14*, 1128.
(42) Lyons, R. G. *Understanding Digital Signal Processing*; Pearson Education, 2011; pp 135−158.
(43) Thomson, G. W. The Antoine Equation for Vapor-pressure Data. *Chem. Rev.* **1946**, *38*, 1.
(44) Gordon, I. E.; et al. The HITRAN2016 Molecular Spectroscopic Database. *J. Quant. Spectrosc. Radiat. Transfer* **2017**, *203*, 3.
(45) Hoshina, H.; et al. Precise measurement of pressure broadening parameters for water vapor with a terahertz time-domain spectrometer. *J. Quant. Spectrosc. Radiat. Transfer* **2008**, *109*, 2303.
(46) Rothman, L. S.; et al. The HITRAN Molecular Spectroscopic Database and HAWKS (HITRAN Atmospheric Workstation): 1996 Edition. *J. Quant. Spectrosc. Radiat. Transfer* **1998**, *60*, 665.
(47) Boyd, R. W. *Nonlinear Optics*; Elsevier, 2008; pp 375−377.
(48) Tennyson, J.; et al. IUPAC critical evaluation of the rotational−vibrational spectra of water vapor, Part III: Energy levels and transition wavenumbers for H216O. *J. Quant. Spectrosc. Radiat. Transfer* **2013**, *117*, 29.
(49) Carlon, H. R. Do clusters contribute to the infrared absorption spectrum of water vapor? *Infrared Phys.* **1979**, *19*, 549.
(50) Carlon, H. R. Infrared absorption by molecular clusters in water vapor. *J. Appl. Phys.* **1981**, *52*, 3111.
(51) Johnson, K.; et al. Water vapor: An extraordinary terahertz wave source under optical excitation. *Phys. Lett. A* **2008**, *372*, 6037.
(52) Dai, Z.; Su, Q.; Lu, D.; Sun, L.; Liu, W. A combined experimental and theoretical study on the terahertz vibrations of water vapors. *Spectrochim. Acta, Part A* **2019**, *214*, 277.

https://doi.org/10.1021/acsphotonics.1c00056
ACS Photonics 2021, 8, 1683−1688